A posterior error estimate for an iterative scheme associated to the Darcy-Forchheimer problem with pressure boundary condition

RIM ALDBAISSY[1], TONI SAYAH[2]
[1]Faculty of engineering (ESIB), Saint Joseph University of Beirut,
LEBANON
[2]Laboratoire de Mathématiques et Applications, URMM, CAR,
Faculté des Sciences, Université Saint-Joseph de Beyrouth,
B.P 11-514 Riad El Solh, Beyrouth 1107 2050,
LEBANON

Abstract: This paper investigates the *a posteriori* error estimates associated with the Darcy–Forchheimer problem under pressure boundary conditions. The problem is discretized using finite element methods and an iterative scheme is recalled along with its corresponding convergence properties. We then derive *a posteriori* error estimates, where the error between the exact and approximate solutions is bounded by two types of indicators: one related to the discretization and the other to the iteration process. Finally, we present several numerical experiments using the adaptive mesh method to highlight the effectiveness of the proposed approach.

Key-Words: Darcy-Forchheimer problem, Finite element method, Iterative scheme, *A posteriori* error estimate.
Received: March 16, 2025. Revised: July 11, 2025. Accepted: August 5, 2025. Published: October 9, 2025.

1 Introduction

The Darcy–Forchheimer model generalizes Darcy's law to account for nonlinear inertial effects in fluid flow through porous media. This results in the following system of partial differential equations posed on a bounded Lipschitz domain $\Omega \subset \mathbb{R}^d$ ($d = 2$ or 3):

$$\frac{\mu}{\rho} K^{-1}\mathbf{u} + \frac{\beta}{\rho}|\mathbf{u}|\mathbf{u} + \nabla p = \mathbf{f}, \tag{1}$$

along with the divergence constraint

$$\operatorname{div} \mathbf{u} = b \quad \text{in} \quad \Omega, \tag{2}$$

and an homogeneous pressure boundary condition

$$p = 0 \quad \text{on} \ \partial\Omega. \tag{3}$$

While the homogeneous boundary condition (3) can readily be generalized to the non-homogeneous case ($p = g_p$ on $\partial\Omega$), we adopt (3) here for the sake of simplicity.

Here, $\mathbf{u}$ denotes the velocity field, p the pressure, K the permeability tensor, and μ and ρ the viscosity and density of the fluid, respectively. The coefficient $\beta > 0$ is the Forchheimer number, which accounts for inertial effects on the flow. The terms $\mathbf{f}$ and b represent, respectively, body forces and fluid sources or sinks. The notation $|\mathbf{u}|$ refers to the Euclidean norm, i.e., $|\mathbf{u}|^2 = \mathbf{u}\cdot\mathbf{u}$. The tensor K in (1) is assumed to be uniformly positive definite and bounded, with the following properties:

$$0 < K_m\, \mathbf{x}\cdot\mathbf{x} \le (K^{-1}(\mathbf{x})\mathbf{x})\cdot\mathbf{x} \le K_M\, \mathbf{x}\cdot\mathbf{x}, \tag{4}$$

where $K_m > 0$ and $K_M > 0$.

In all the rest of this paper, we denote by Problem (P) the system of equations (1), (2) and (3).

In an early contribution to the Darcy–Forchheimer literature, [1], introduced a mixed finite element formulation that accommodates non-homogeneous boundary conditions on the normal component of the velocity. They proved the existence and uniqueness of the corresponding weak solution and developed a discrete scheme using piecewise constants for the velocity and Crouzeix–Raviart elements for the pressure. To address the nonlinearity of the resulting algebraic system, they proposed and analyzed an alternating directions iterative algorithm, providing convergence results and *a priori* error estimates. These theoretical results were later validated through numerical experiments by [2], who also proposed an alternative mixed element pair yielding smoother pressure approximations. Since then, several studies have extended and refined finite element approaches for solving the Darcy–Forchheimer equation, from both theoretical and computational perspectives. Furthermore, in [3], the Darcy–Forchheimer system was coupled with the concentration equation. The existence and uniqueness of solutions were demonstrated via a Galerkin method, after which finite element discretization was applied and optimal *a priori* error estimates were derived.

Building upon these works, the authors in [4],

considered the Darcy–Forchheimer model with pressure boundary conditions and proposed a mixed finite element discretization using Raviart–Thomas and Brezzi–Douglas–Marini elements. They demonstrated the existence and uniqueness of weak solutions and provided associated error estimates, though the convergence of their proposed iterative algorithm was not fully explored. A more detailed theoretical analysis of the finite element spaces introduced in [2], was later provided by [5], including proofs of convergence and the derivation of *a priori* error estimates. In [6], we introduced an iterative scheme for the Darcy–Forchheimer problem with pressure boundary conditions and studied its corresponding well-posedness and convergence.

Regarding the *a posteriori* analysis, various extensions of the Darcy–Forchheimer model have been studied. In [7], the coupling of the Navier–Stokes and Darcy–Forchheimer systems was investigated. In [8], *a posteriori* error bounds were derived for the Brinkman–Darcy–Forchheimer problem. The *a posteriori* error estimates for the Darcy–Forchheimer problem with normal velocity boundary conditions were studied in [9]. This latter contribution was extended in [10], to analyze the *a posteriori* error bounds for the Darcy–Forchheimer problem (as treated in [9]) coupled with a convection–diffusion–reaction equation.

A wide range of recent studies have addressed the Darcy–Forchheimer equation from both theoretical and applied perspectives. For theoretical developments and numerical analysis, we refer to [11], [12], [13], [14], [15], [16], [17], [18], [19] and [20]. Regarding practical applications, relevant contributions can be found in [21], [22], [23],[24], [25], and, [26].

In this paper, we consider the Darcy–Forchheimer problem with pressure boundary conditions, as treated in [6], and recall the iterative scheme introduced there along with its convergence analysis. We then establish *a posteriori* error estimates and carry out two-dimensional numerical investigations using the adaptive mesh method. The novelty of this work lies in the derived *a posteriori* error estimates for the Darcy–Forchheimer problem with pressure boundary conditions and in the corresponding numerical experiments based on the adaptive mesh method.

The structure of this paper is as follows:

- Section 2 describes the problem and the weak formulation.
- Section 3 delves into the discretization process and explores the convergence of the proposed iterative scheme.
- Section 4 presents the results of our numerical simulations.

2 Notations and weak formulations

To formulate the weak problem and analyze its numerical approximation, we begin by introducing the functional framework and the notations used throughout this work.
For a multi-index $\alpha = (\alpha_1, \ldots, \alpha_d) \in \mathbb{N}^d$, we denote $|\alpha| = \alpha_1 + \cdots + \alpha_d$, and define the mixed partial derivative:

$$\partial^\alpha = \frac{\partial^{|\alpha|}}{\partial x_1^{\alpha_1} \cdots \partial x_d^{\alpha_d}}.$$

Given an integer $m \geq 0$ and a real $q \geq 1$, we define the Sobolev space

$$W^{m,q}(\Omega) = \{v \in L^q(\Omega); \\ \partial^\alpha v \in L^q(\Omega) \text{ for all } |\alpha| \leq m\},$$

equipped with the following norm and seminorm

$$\|v\|_{W^{m,q}(\Omega)} = \left(\sum_{|\alpha|\leq m} \|\partial^\alpha v\|^q_{L^q(\Omega)}\right)^{1/q},$$
$$|v|_{W^{m,q}(\Omega)} = \left(\sum_{|\alpha|=m} \|\partial^\alpha v\|^q_{L^q(\Omega)}\right)^{1/q}.$$

In the case $q = 2$, this space coincides with the Hilbert space $H^m(\Omega)$. The inner product in $L^2(\Omega)$ is denoted by $(\cdot, \cdot)$.
For vector-valued functions $\mathbf{v} : \Omega \to \mathbb{R}^d$, the corresponding L^q-norm is defined as

$$\|\mathbf{v}\|_{L^q(\Omega)} = \left(\int_\Omega |\mathbf{v}(x)|^q \, dx\right)^{1/q},$$

where $|\cdot|$ denotes the Euclidean norm in $\mathbb{R}^d$.

To proceed with the analysis of Problem (P), we first introduce the appropriate function spaces and notation used throughout this section. Detailed properties and justifications of the variational setting can be found in [4].
We define the pressure space as $M = L^2(\Omega)$ and the velocity space as

$$X = \left\{\mathbf{v} \in L^3(\Omega)^d \ : \ \operatorname{div}(\mathbf{v}) \in L^2(\Omega)\right\},$$

equipped with the norm

$$\|\mathbf{v}\|_X = \|\mathbf{v}\|_{L^3(\Omega)} + \|\operatorname{div}(\mathbf{v})\|_{L^2(\Omega)}.$$

It is known that these spaces satisfy the classical inf-sup condition: There exists a constant $\gamma > 0$ such that

$$\inf_{q \in M} \sup_{\mathbf{v} \in X} \frac{\int_\Omega q \ \mathrm{div}(\mathbf{v}) \, d\mathbf{x}}{\|q\|_M \|\mathbf{v}\|_X} \geq \gamma. \tag{5}$$

In this study, the source term $\mathbf{f}$ is taken to be the gradient of a scalar field $Z \in H^1(\Omega)$, i.e., $\mathbf{f} = \nabla Z \in L^2(\Omega)^d$, and we assume that $b \in L^2(\Omega)$ (see, [4], for a detailed discussion of these assumptions).

To formulate the weak problem, we introduce the nonlinear operator $\mathcal{A} : L^3(\Omega)^d \to L^{3/2}(\Omega)^d$ defined as follows:

$$\mathcal{A}(\mathbf{v}) = \frac{\mu}{\rho} K^{-1} \mathbf{v} + \frac{\beta}{\rho} |\mathbf{v}| \mathbf{v}.$$

The operator $\mathcal{A}$ exhibits the following key monotonicity properties (see, [1],[27]):

Property 2.1. *Let* $\mathbf{v}, \mathbf{w} \in L^3(\Omega)^d$. *Then:*

1. *Positivity:*

$$\frac{\mu}{\rho} \int_\Omega K^{-1} \mathbf{v} \cdot \mathbf{v} \, d\mathbf{x} \geq \frac{\mu K_m}{\rho} \|\mathbf{v}\|^2_{L^2(\Omega)}.$$

2. *Strict monotonicity:*

$$\frac{\beta}{\rho} \int_\Omega (|\mathbf{v}|\mathbf{v} - |\mathbf{w}|\mathbf{w}) \cdot (\mathbf{v} - \mathbf{w}) \, d\mathbf{x} \geq c_m \|\mathbf{v} - \mathbf{w}\|^3_{L^3(\Omega)},$$

where $c_m > 0$ *is a constant depending on* $|\Omega|$.

Using these definitions, Problem (P) can be equivalently expressed in variational form: Find $(\mathbf{u}, p) \in X \times M$ such that

$$\begin{cases} \forall \mathbf{v} \in X, & \displaystyle\int_\Omega \mathcal{A}(\mathbf{u}) \, \mathbf{v} \, d\mathbf{x} - \int_\Omega p \ \mathrm{div}(\mathbf{v}) \, d\mathbf{x} \\ & \qquad = \displaystyle\int_\Omega \mathbf{f} \, \mathbf{v} \, d\mathbf{x}, \\ \forall q \in M, & \displaystyle\int_\Omega q \ \mathrm{div}(\mathbf{u}) \, d\mathbf{x} = \int_\Omega b \, q \, d\mathbf{x}. \end{cases} \tag{6}$$

As shown in [4], the variational problem (6) admits a unique solution $(\mathbf{u}, p) \in X \times M$ satisfying the following *a priori* bounds: There exists a positive constant C such that,

$$\begin{aligned} &||\mathbf{u}||^2_{L^2(\Omega)} + ||\mathbf{u}||^3_{L^3(\Omega)} + ||\,\mathrm{div}(\mathbf{u})||^2_{L^2(\Omega)} \\ &\qquad \leq C(||b||^2_{L^2(\Omega)} + ||b||^3_{L^2(\Omega)} + ||\mathbf{f}||^2_{L^2(\Omega)}), \\ &||p||_{L^2(\Omega)} \leq C(||b||_{L^2(\Omega)} + ||b||^2_{L^2(\Omega)} + ||\mathbf{f}||_{L^2(\Omega)} \\ &\qquad + ||\mathbf{f}||^2_{L^2(\Omega)}). \end{aligned} \tag{7}$$

3 Finite Element Discretization

To proceed with the numerical approximation of Problem (P), we assume that the domain Ω is polygonal when $d = 2$ and polyhedral when $d = 3$, ensuring that it can be completely partitioned by a mesh. We consider a family of shape-regular triangulations $(\mathcal{T}_h)_h$ of Ω, as described in [28]. Each triangulation $\mathcal{T}_h$ consists of closed, non-degenerate simplices-triangles for $d = 2$ and tetrahedra for $d = 3$-referred to as elements, and must satisfy the following conditions:

- For any h, the closure $\bar{\Omega}$ is exactly covered by the union of all elements in $\mathcal{T}_h$;
- Any two distinct elements in $\mathcal{T}_h$ intersect either at a common vertex, along a shared edge (when $d = 2$), along a shared face (when $d = 3$), or not at all;
- There exists a constant $\sigma > 0$, independent of h, such that for all $\kappa \in \mathcal{T}_h$, the ratio between the element diameter h_κ and the radius ρ_κ of the largest inscribed circle (in 2D) or ball (in 3D) is bounded:

$$\max_{\kappa \in \mathcal{T}_h} \frac{h_\kappa}{\rho_\kappa} \leq \sigma. \tag{8}$$

As is standard, we denote by h the maximum diameter among all elements of $\mathcal{T}_h$.
Let r be a non-negative integer. For each element κ in the mesh $\mathcal{T}_h$, we denote by $\mathbb{P}_r(\kappa)$ the space of polynomials of total degree at most r in d variables, restricted to κ. The same notation is used for the faces or edges of κ. For each edge (when $d = 2$) or face (when $d = 3$), we denote by h_e the diameter of e.
In order to apply inverse inequalities, we further assume that the triangulations are uniformly regular. That is, there exists a constant $\beta_0 > 0$ such that for every $\kappa \in \mathcal{T}_h$, we have

$$h_\kappa \geq \beta_0 h.$$

We will use the following standard inverse inequalities: for any $0 < p \leq q$, in arbitrary spatial dimension d, and for polynomial functions v_h of degree r, there exist constants $C_I(p, q)$ and $C_J(q)$ such that for any element κ and for any edge (if $d = 2$) or face (if $d = 3$) e of the triangulation $\mathcal{T}_h$ (see, [29],

$$\begin{aligned} &\|v_h\|_{L^q(\kappa)} \leq C_I(p, q) h_\kappa^{\frac{d}{p} - \frac{d}{q}} \|v_h\|_{L^p(\kappa)} \\ &\text{and} \\ &\|v_h\|_{L^q(e)} \leq C_J(q) h_e^{\frac{d-1}{q} - \frac{d-1}{2}} \|v_h\|_{L^p(e)}. \end{aligned} \tag{9}$$

The constants C_I and C_J may depend on the shape regularity parameter σ defined in (8). In the remainder of the manuscript, we will not explicitly indicate this dependence to simplify notation.

3.1 Discretization of the variational problem

To approximate the solution of Problem (6), we begin by discretizing the variational formulation using the strategy presented in [4], where the authors introduced a discrete formulation based on mixed finite elements, including the Raviart–Thomas element, [30], and the Brezzi–Douglas–Marini element, [31]. Although an iterative scheme was proposed in their work, its convergence was not analyzed. Numerical simulations were also provided to support their approach.

In what follows, we consider the Raviart–Thomas $RT0$ mixed finite element space, [30], defined by:

$$\begin{aligned} X_h =&\{\mathbf{v}_h \in X;\ \mathbf{v}_h(\mathbf{x})|_\kappa = a_\kappa \mathbf{x} + \mathbf{b}_\kappa, a_\kappa \in \mathbb{R}, \\ &\mathbf{b}_\kappa \in \mathbb{R}^d, \forall\, \kappa \in \mathcal{T}_h\}, \\ M_h =&\{q_h \in L^2(\Omega);\ \forall\, \kappa \in \mathcal{T}_h,\ q_h|_\kappa \text{ is constant}\}. \end{aligned} \tag{10}$$

These spaces satisfy the following discrete inf-sup condition:

$$\forall, q_h \in M_h, ;\ \sup_{\mathbf{v}_h \in X_h} \frac{\displaystyle\int_\Omega q_h \,\mathrm{div}(\mathbf{v}_h) d\mathbf{x},}{||\mathbf{v}_h||_X} \geq \beta_p ||q_h||_{M_h}, \tag{11}$$

where β_p is a positive constant independent of the mesh size h.

Problem (6) can then be discretized as follows:

$$\begin{cases} \forall \mathbf{v}_h \in X_h, \quad \dfrac{\mu}{\rho}\displaystyle\int_\Omega K^{-1}\mathbf{u}_h \mathbf{v}_h \, d\mathbf{x} \\ \qquad + \dfrac{\beta}{\rho}\displaystyle\int_\Omega |\mathbf{u}_h|\mathbf{u}_h \mathbf{v}_h \, d\mathbf{x} - \int_\Omega p_h \ \mathrm{div}(\mathbf{v}_h)\, d\mathbf{x} \\ \qquad = \displaystyle\int_\Omega \mathbf{f}\,\mathbf{v}_h \, d\mathbf{x}, \\ \forall q_h \in M_h, \quad \displaystyle\int_\Omega q_h \ \mathrm{div}(\mathbf{u}_h)\, d\mathbf{x} = \int_\Omega b q_h \, d\mathbf{x}. \end{cases} \tag{12}$$

It is also shown in [4], that there exists a unique $\mathbf{u}_{h,p} \in X_h$ such that:

$$\forall q_h \in M_h, \quad \int_\Omega q_h \ \mathrm{div}(\mathbf{u}_{h,p}) d\mathbf{x} = \int_\Omega b\, q_h d\mathbf{x}, \tag{13}$$

and this velocity field satisfies the estimate:

$$||\mathbf{u}_{h,p}||_X \leq C_{l2} ||b||_{L^2(\Omega)}. \tag{14}$$

In [4], the authors proved that Problem (12) admits a unique solution $(\mathbf{u}_h, p_h) \in X_h \times M_h$, which satisfies the same type of bounds as those established in (7). Furthermore, the continuous solution $(\mathbf{u}, p)$ of (6) and the discrete solution $(\mathbf{u}_h, p_h)$ of (12) satisfy the following *a priori* error estimate:

Theorem 3.1. *Let $(\mathbf{u}_h, p_h)$ be the solution of Problem* (12)*. If the solution of Problem* (6) *is such that $(\mathbf{u}, p) \in W^{1,3}(\Omega)^d \times W^{1,3/2}(\Omega)$, then there exists a constant C independent of h such that*

$$\begin{aligned} &||\mathbf{u} - \mathbf{u}_h||^2_{L^2(\Omega)} + ||\mathbf{u} - \mathbf{u}_h||^3_{3,\Omega} \leq Ch^2, \\ &||p - p_h||_{L^2(\Omega)} \leq Ch. \end{aligned} \tag{15}$$

Next, we recall an iterative scheme introduced in [4], described as follows: for a given initial guess $\mathbf{u}_h^0 \in X_h$ and having $\mathbf{u}_h^i$ at each iteration i, we compute $(\mathbf{u}_h^{i+1}, p_h^{i+1})$ solution of

$$\begin{cases} \forall \mathbf{v}_h \in X_h, \quad \alpha \displaystyle\int_\Omega (\mathbf{u}_h^{i+1} - \mathbf{u}_h^i)\mathbf{v}_h \\ + \dfrac{\mu}{\rho}\displaystyle\int_\Omega K^{-1}\mathbf{u}_h^{i+1}\mathbf{v}_h \, d\mathbf{x} + \dfrac{\beta}{\rho}\int_\Omega |\mathbf{u}_h^i|\mathbf{u}_h^{i+1}\mathbf{v}_h \, d\mathbf{x} \\ - \displaystyle\int_\Omega p_h^{i+1} \ \mathrm{div}(\mathbf{v}_h)\, d\mathbf{x} = \int_\Omega \mathbf{f}\,\mathbf{v}_h \, d\mathbf{x}, \\ \forall q_h \in M_h, \quad \displaystyle\int_\Omega q_h \ \mathrm{div}(\mathbf{u}_h^{i+1})\, d\mathbf{x} = \int_\Omega b\, q_h \, d\mathbf{x}, \end{cases} \tag{16}$$

where α is a given positive parameter.

In the following, we recall two theorems introduced and showed in [4], concerning the convergence of the iterative algorithm (16) when α is sufficiently large and the initial guess $\mathbf{u}_h^0$ is sufficiently close to $\mathbf{u}_{h,p}$.

Theorem 3.2. *Problem* (16) *admits a unique solution $(\mathbf{u}_h^{i+1}, p_h^{i+1})$ in $X_h \times M_h$. Furthermore, if the initial value $\mathbf{u}_h^0$ satisfies the condition*

$$||\mathbf{u}_h^0 - \mathbf{u}_{h,l}||_{L^2(\Omega)} \leq L_1(\mathbf{f}, \mathbf{u}_{h,p}), \tag{17}$$

where

$$\begin{aligned} L_1(\mathbf{f}, \mathbf{u}_{h,p}) = \Big(&\tfrac{2\rho}{\mu K_m}\big(\tfrac{3\rho}{2\mu K_m}||\mathbf{f}||^2_{L^2(\Omega)} \\ &+ (\tfrac{\mu K_m}{6\rho} + \tfrac{3\mu K_M^2}{2\rho K_m})||\mathbf{u}_{h,p}||^2_{L^2(\Omega)} \\ &+ \tfrac{4\beta}{3\rho}||\mathbf{u}_{h,p}||^3_{L^3(\Omega)}\big)\Big)^{1/2} \end{aligned} \tag{18}$$

and if α satisfies the condition

$$\begin{aligned} \alpha > 2\big(&\tfrac{3\beta^2}{\rho\mu K_m} C_I^4 h^{-\frac{2d}{3}} ||\mathbf{u}_{h,p}||^2_{L^3(\Omega)} \\ &+ \tfrac{4\beta}{3\rho} C_I^3 h^{-d/2} L_2(\mathbf{f}, L_1(\mathbf{f}, \mathbf{u}_{h,p}))^2\big), \end{aligned} \tag{19}$$

where

$$L_2(\mathbf{f},\eta)=\frac{\rho}{\mu K_m}\big(\|\mathbf{f}\|_{L^2(\Omega)^d}+\frac{\mu K_M}{\rho}\|\mathbf{u}_{h,p}\|_{L^2(\Omega)}$$
$$+\frac{\beta}{\rho}c_I^3h^{-\frac{d}{2}}\|\mathbf{u}_{h,p}\|^2_{L^2(\Omega)}+\frac{\mu K_M}{\rho}\eta+\frac{\beta}{\rho}c_I^3h^{-\frac{d}{2}}\eta^2\big).$$

then the solution of Problem (16) *satisfies the estimates*

$$||\mathbf{u}_h^{i+1}-\mathbf{u}_{h,p}||_{L^2(\Omega)}\leq L_1(\mathbf{f},\mathbf{u}_{h,p}), \quad (20)$$

$$||\mathbf{u}_h^{i+1}||_{L^2(\Omega)}\leq L_1(\mathbf{f},\mathbf{u}_{h,p})+||\mathbf{u}_{h,p}||_{L^2(\Omega)}, \quad (21)$$

and

$$||\mathbf{u}_h^{i+1}||^3_{L^3(\Omega)}\leq(\frac{3\mu K_m}{2\beta}+\frac{3\alpha\rho}{2\beta})L_1^2(\mathbf{f},\mathbf{u}_{h,p}). \quad (22)$$

Remark 3.3. *In Theorem 3.2, we show convergence when the initial guess* $\mathbf{u}_h^0$ *lies within a ball centered at* $\mathbf{u}_{h,p}$ *with radius* $L_1(\mathbf{f},\mathbf{u}_{h,p})$*, which is unknown. However, the expression of* $L_1(\mathbf{f},\mathbf{u}_{h,p})$ *shows that the initial guess* $\mathbf{u}_h^0=\mathbf{0}$ *satisfies Relation* (17)*.*

The next theorem addresses the convergence of the solution of the iterative problem (16).

Theorem 3.4. *Under the assumptions of Theorem* 3.2 *and if* α *is such that*

$$\alpha>\frac{\rho C^2}{K_m\mu}h^{-d} \quad (23)$$

where

$$C=\frac{\beta}{\rho}C_I^3\big(L_1(\mathbf{f},\mathbf{u}_{h,l})+\|\mathbf{u}_{h,l}\|_{L^2(\Omega)}\big),$$

then the iterative solutions $(\mathbf{u}_h^i,p_h^i)$ *of Problem* (16) *converges in* $L^2(\Omega)^d\times L^2(\Omega)$ *to the solution* $(\mathbf{u}_h,p_h)$ *of Problem* (12)*.*

Remark 3.5. *To establish the convergence of the algorithm* (16)*, the assumptions of Theorems 3.2 and 3.4 necessitate conditions* (19) *and* (23)*. In [6], we investigated how the convergence of the iterative scheme* (16) *depends on the parameter* α *in specific scenarios.*

4 A posteriori error estimates

As is standard in the context of *a posteriori* error estimation, we begin by introducing the following notation. Let us denote by

- Γ_h^i the set of edges (when $d=2$) or faces (when $d=3$) of κ that are not contained in $\partial\Omega$.
- Γ_h^b the set of edges (when $d=2$) or faces (when $d=3$) of κ which are contained in $\partial\Omega$.

For every element $\kappa\in\mathcal{T}_h$, we denote by $w\kappa$ the union of elements $K\in\mathcal{T}_h$ such that $\kappa\cap K\neq\emptyset$. Furthermore, for every edge (when $d=2$) or face (when $d=3$) e of the mesh $\mathcal{T}_h$, we denote by:

- ω_e the union of elements in $\mathcal{T}_h$ adjacent to e;
- $[\cdot]_e$ the jump across $e\in\Gamma_h^i$.

From this point onward, we also assume that $b\in L^2(\Omega)$.

This section, along with the next, establishes *a posteriori* error estimates under the assumption of slightly higher regularity for the solution.

Let R_h denote a Clément-type interpolation operator (see, [32]). The following interpolation error estimates hold (see, for example, [9]): for all κ in $\mathcal{T}_h$, for all e in $\partial\kappa$ and for all $q\in W^{1,p}(\Omega)$,

$$\|q-R_hq\|_{L^p(\kappa)}\leq Ch_\kappa|q|_{W^{1,p}(w_\kappa)} \quad (24)$$

and

$$\|q-R_hq\|_{L^p(e)}\leq Ch_e^{1-1/p}|q|_{W^{1,p}(w_e)}, \quad (25)$$

where C denotes a constant independent of the mesh size h.

4.0.1 Upper error bound

To derive upper bounds, we begin by formulating the residual equation.
A straightforward computation shows that the solutions of problems (6) and (16) satisfy, for all $(\mathbf{v},q)\in X\times M$ and $(\mathbf{v}_h,q_h)\in X_h\times M_h$, the

following:

$$\begin{aligned}
&\frac{\mu}{\rho}\int_\Omega K^{-1}(\mathbf{u}-\mathbf{u}_h^{i+1})\mathbf{v}\,d\mathbf{x}-\int_\Omega (p-p_h^{i+1})\,\mathrm{div}\,\mathbf{v}\,d\mathbf{x}\\
&+\frac{\beta}{\rho}\int_\Omega (|\mathbf{u}|\mathbf{u}-|\mathbf{u}_h^i|\mathbf{u}_h^{i+1})\mathbf{v}\,d\mathbf{x}\\
&=\sum_{\kappa\in\mathcal{T}_h}\Big[\int_\kappa(-\alpha(\mathbf{u}_h^{i+1}-\mathbf{u}_h^i)-\frac{\mu}{\rho}K^{-1}\mathbf{u}_h^{i+1}\\
&\qquad -\frac{\beta}{\rho}|\mathbf{u}_h^{i+1}|\mathbf{u}_h^{i+1}+\mathbf{f}_h)(\mathbf{v}-\mathbf{v}_h)\,d\mathbf{x}\Big]\\
&+\int_\Omega p_h^{i+1}\,\mathrm{div}(\mathbf{v}-\mathbf{v}_h)d\mathbf{x}\\
&+\sum_{\kappa\in\mathcal{T}_h}\Big[\int_\kappa(\mathbf{f}-\mathbf{f}_h)(\mathbf{v}-\mathbf{v}_h)\,d\mathbf{x}\\
&\qquad +\alpha\int_\kappa(\mathbf{u}_h^{i+1}-\mathbf{u}_h^i)\mathbf{v}\,d\mathbf{x}\\
&\qquad +\frac{\beta}{\rho}\int_\kappa(|\mathbf{u}_h^{i+1}|-|\mathbf{u}_h^i|)\mathbf{u}_h^{i+1}(\mathbf{v}-\mathbf{v}_h)\Big]
\end{aligned}\tag{26}$$

and

$$\begin{aligned}
\int_\Omega q\;\mathrm{div}(\mathbf{u}-\mathbf{u}_h^{i+1})\,d\mathbf{x}&=\int_\Omega(b-b_h)\,(q-q_h)\,d\mathbf{x}\\
&+\int_\Omega(b_h-\mathrm{div}(\mathbf{u}_h^{i+1}))\,(q-q_h)\,d\mathbf{x},
\end{aligned}\tag{27}$$

where $\mathbf{f}_h$ denotes a polynomial approximation of $\mathbf{f}$, and b_h is an approximation of b that is constant on each element κ of the mesh $\mathcal{T}_h$.

Based on the error equations (26) and (27), we define the following error indicators associated with each element $\kappa\in\mathcal{T}_h$:

$$\begin{aligned}
\eta_{\kappa,i}^{(L)} &= ||\mathbf{u}_h^{i+1}-\mathbf{u}_h^i||_{L^2(\kappa)},\\
\eta_{\kappa,i}^{(D_1)} &= \|\mathbf{f}_h-\alpha(\mathbf{u}_h^{i+1}-\mathbf{u}_h^i)-\frac{\mu}{\rho}K^{-1}\mathbf{u}_h^{i+1}\\
&\qquad -\frac{\beta}{\rho}|\mathbf{u}_h^{i+1}|\mathbf{u}_h^{i+1}-\nabla p_h^{i+1}\,\|_{L^2(\kappa)}\\
&\qquad +\frac{1}{2}\sum_{e\in\partial\kappa}h_e^{\frac{1}{2}}\|[p_h^{i+1}\mathbf{n}]\|_{L^2(e)}\\
\eta_{\kappa,i}^{(D_2)} &= \|b_h-\mathrm{div}(\mathbf{u}_h^{i+1}))\|_{L^2(\kappa)}.
\end{aligned}\tag{28}$$

We mention that p_h^{i+1} is constant on each triangle $\kappa\in\mathcal{T}_h$, then we have $\nabla p_h^{i+1}=\mathbf{0}$ on each κ, but we keep it in the indicators $\eta_{\kappa,i}^{(D_1)}$ for the shape of the indicators of discretization corresponding to the Darcy Forchheimer equation.

To derive an *a posteriori* error estimate, it is necessary to establish bounds for the numerical solutions $\mathbf{u}_h$ of Problem (12) and $\mathbf{u}_h^{i+1}$ of (16) in the $L^6(\Omega)$ norm. This is the focus of the following lemma.

Lemma 4.1. *Under the assumptions of Theorem 3.1 and assume that* $\mathbf{u}\in W^{1,6}(\Omega)$*, the solution* $\mathbf{u}_h$ *of Problem* (12) *satifies the follwonig bound*

$$\|\mathbf{u}_h\|_{L^6(\Omega)}\le C_1(\mathbf{u},p),\tag{29}$$

where C_1 *is a positive constant independent on* h *but depends on the exact solution* $(\mathbf{u},p)$ *of* (6).
Furthermore, under the assumptions of the theorems 3.2 and 3.4, there exists an integer i_0 *depending on* h *such that for all* $i\ge i_0$*, the solution* $\mathbf{u}_h^{i+1}$ *of* (16) *verifies the following bound:*

$$\|\mathbf{u}_h^{i+1}\|_{L^6(\Omega)}\le C_2(\mathbf{u},p),\tag{30}$$

where C_2 *is a positive constant independent of* h *but depends on the exact solution* $(\mathbf{u},p)$ *of* (6).

Proof. Let $(\mathbf{u},p)$ be the solution of (6), $(\mathbf{u}_h,p_h)$ be the solution of (12) and $(\mathbf{u}_h^{i+1},p_h^{i+1})$ be the solution of (16).
By using (9) (for $p=6,q=3$), $\mathbf{u}_h$ can be bounded as follows:

$$\begin{aligned}
\|\mathbf{u}_h\|_{L^6(\Omega)}&\le\|\mathbf{u}_h-R_h\mathbf{u}\|_{L^6(\Omega)}\\
&\qquad+\|R_h\mathbf{u}-\mathbf{u}\|_{L^6(\Omega)}+\|\mathbf{u}\|_{L^6(\Omega)}\\
&\le Ch^{-d/6}\|\mathbf{u}_h-R_h\mathbf{u}\|_{L^3(\Omega)}\\
&\qquad+\|R_h\mathbf{u}-\mathbf{u}\|_{L^6(\Omega)}+\|\mathbf{u}\|_{L^6(\Omega)}\\
&\le Ch^{-d/6}(\|\mathbf{u}_h-\mathbf{u}\|_{L^3(\Omega)}+\|R_h\mathbf{u}-\mathbf{u}\|_{L^3(\Omega)})\\
&\qquad+\|R_h\mathbf{u}-\mathbf{u}\|_{L^6(\Omega)}+\|\mathbf{u}\|_{L^6(\Omega)}.
\end{aligned}\tag{31}$$

Next, we use the bound (15) and the properties (24) of the operator R_h to obtain

$$\|\mathbf{u}_h\|_{L^6(\Omega)}\le C_1(\mathbf{u},p).\tag{32}$$

We now proceed to establish the bound (30). Applying the inverse inequality (9) with $q=6$ and $p=2$, together with the bound (32), we obtain the following estimate for $|\mathbf{u}^{i+1}h|L^6(\Omega)$:

$$\begin{aligned}
\|\mathbf{u}_h^{i+1}\|_{L^6(\Omega)} &\le \|\mathbf{u}_h^{i+1}-\mathbf{u}_h\|_{L^6(\Omega)}+\|\mathbf{u}_h\|_{L^6(\Omega)}\\
&\le C\big(h^{-d/3}\|\mathbf{u}_h^{i+1}-\mathbf{u}_h\|_{L^2(\Omega)}\\
&\qquad+C_1(\mathbf{u},p)\big).
\end{aligned}\tag{33}$$

As $\mathbf{u}_h^{i+1}$ converges to $\mathbf{u}_h$ in $L^2(\Omega)$, there exists an integer i_0 depending on h such that for all $i \geq i_0$ we have

$$\|\mathbf{u}_h^{i+1} - \mathbf{u}_h\|_{L^2(\Omega)} \leq h^{d/3}. \tag{34}$$

Then, Equation (33) gives by using (34) the following bound for all $i \geq i_0$:

$$\|\mathbf{u}_h^{i+1}\|_{L^6(\Omega)} \leq \widehat{C}(\mathbf{u}, p). \tag{35}$$

Hence, we get the desired results. □

Our objective is to derive an upper bound for the error between the exact solution $(\mathbf{u}, p)$ of (6) and the numerical approximation $(\mathbf{u}_h^{i+1}, p_h^{i+1})$ obtained from the iterative scheme (16). To this end, we begin with the following lemma, which is a consequence of the inf-sup condition (5).

Lemma 4.2. *There exists a velocity $\mathbf{v}_r$ in X that solves the following equation : $\forall q \in M$,*

$$\begin{aligned}\int_\Omega q\,\mathrm{div}(\mathbf{v}_r)\,d\mathbf{x} &= \int_\Omega (b - b_h)\,q\,d\mathbf{x} \\ &+ \int_\Omega (b_h - \mathrm{div}\ \mathbf{u}_h^{i+1})\,q\,d\mathbf{x}\end{aligned} \tag{36}$$

satisfying the following bound

$$\|\mathbf{v}_r\|_X \quad \leq \quad \hat{C}_2 \sum_{\kappa\in\mathcal{T}_h} \big(\eta_{\kappa,i}^{(D_2)} + ||b - b_h||_{L^3(\kappa)}\big). \tag{37}$$

Proof. Equation (27) with $q_h = 0$ and the inf-sup condition (5) imply that there exists a $\mathbf{v}_r \in X$ such that (36) is verified and satisfying

$$\begin{aligned}\|\mathbf{v}_r\|_X &\leq C \sup_{q\in M} \tfrac{1}{\|q\|_M} \sum_{\kappa\in\mathcal{T}_h} \Big[\int_\kappa q(-b + b_h)\,d\mathbf{x} \\ &\qquad - \int_\kappa (b_h - \mathrm{div}\ \mathbf{u}_h^{i+1}) q\,d\mathbf{x}\Big] \\ &\leq \hat{C}_2 \sum_{\kappa\in\mathcal{T}_h} \big(\eta_{\kappa,i}^{(D_2)} + \|b - b_h\|_{L^2(\kappa)}\big).\end{aligned} \tag{38}$$

□

Remark 4.3. *the Relations* (36) *and* (27) *(for $q_h = 0$) induce the following relation: $\forall q \in M$,*

$$\int_\Omega q\ \mathrm{div}(\boldsymbol{z}_0) d\mathbf{x} = 0. \tag{39}$$

Theorem 4.4. *Under the assumptions of Lemma 4.1, the solutions $(\mathbf{u}, p)$ of* (6) *and $(\mathbf{u}_h^{i+1}, p_h^{i+1})$ of* (16) *verify the following error inequalities:*

$$\begin{aligned}&\|\mathbf{u} - \mathbf{u}_h^{i+1}\|_{L^2(\Omega)} + \big\|\mathbf{u} - \mathbf{u}_h^{i+1}\big\|_{L^3(\Omega)}^{3/2} + \|\mathbf{v}_r\|_X \\ &\leq C\Big[\sum_{\kappa\in\mathcal{T}_h} \Big(\eta_{\kappa,i}^{(D_1)} + \eta_{\kappa,i}^{(D_2)} + \eta_{\kappa,i}^{(L)}\Big) \\ &\qquad + \sum_{\kappa\in\mathcal{T}_h} \Big(\|\boldsymbol{f} - \boldsymbol{f}_h\|_{L^2(\kappa)} + h_k\|b - b_h\|_{L^3(\kappa)}\Big)\Big],\end{aligned} \tag{40}$$

where $\mathbf{v}_r$ is given in (36)*, C is a constant depending on $\mathbf{u}$ and $\mathbf{f}_h$ (resp. b_h) is an approximation of $\mathbf{f}$ (resp. b) given in* (26) *and* (27)*.*

Proof. The velocity error equation (26) can be written for $\mathbf{v}_h = 0$ as

$$\begin{aligned}&\frac{\mu}{\rho}\int_\Omega K^{-1}(\mathbf{u} - \mathbf{u}_h^{i+1})\mathbf{v}\,d\mathbf{x} - \int_\Omega (p - p_h^{i+1})\,\mathrm{div}\,\mathbf{v}\,d\mathbf{x} \\ &+\frac{\beta}{\rho}\int_\Omega (|\mathbf{u}|\mathbf{u} - |\mathbf{u}_h^{i+1}|\mathbf{u}_h^{i+1})\mathbf{v}\,d\mathbf{x} \\ &= \sum_{\kappa\in\mathcal{T}_h} \Big[\int_\kappa (-\alpha(\mathbf{u}_h^{i+1} - \mathbf{u}_h^i) - \frac{\mu}{\rho}K^{-1}\mathbf{u}_h^{i+1} \\ &\qquad -\frac{\beta}{\rho}|\mathbf{u}_h^{i+1}|\mathbf{u}_h^{i+1} + \mathbf{f}_h)\mathbf{v}\,d\mathbf{x}\Big] \\ &\quad + \int_\Omega p_h^{i+1}\,\mathrm{div}\,\mathbf{v}d\mathbf{x} + \sum_{\kappa\in\mathcal{T}_h}\int_\kappa (\mathbf{f} - \mathbf{f}_h)\mathbf{v}\,d\mathbf{x} \\ &\quad +\alpha \sum_{\kappa\in\mathcal{T}_h}\int_\kappa (\mathbf{u}_h^{i+1} - \mathbf{u}_h^i)\mathbf{v}\,d\mathbf{x}.\end{aligned} \tag{41}$$

Now, to simplify we set $\mathbf{z}_0 = \mathbf{u} - \mathbf{u}_h^{i+1} - \mathbf{v}_r$ and we test the last equation with $\mathbf{v} = \mathbf{z}_0$. By using (39), Relation

(41) reduces to

$$\begin{aligned}
&\frac{\mu}{\rho}\int_\Omega K^{-1}\mathbf{z}_0\mathbf{z}_0\,d\mathbf{x}+\frac{\mu}{\rho}\int_\Omega K^{-1}\mathbf{v}_r\mathbf{z}_0\,d\mathbf{x}\\
&+\frac{\beta}{\rho}\int_\Omega(|\mathbf{u}|\mathbf{u}-|\mathbf{u}_h^{i+1}|\mathbf{u}_h^{i+1})(\mathbf{u}-\mathbf{u}_h^{i+1})\,d\mathbf{x}\\
&-\frac{\beta}{\rho}\int_\Omega(|\mathbf{u}|\mathbf{u}-|\mathbf{u}_h^{i+1}|\mathbf{u}_h^{i+1})\mathbf{v}_r\,d\mathbf{x}\\
&=\sum_{\kappa\in\mathcal{T}_h}\Big[\int_\kappa(-\alpha(\mathbf{u}_h^{i+1}-\mathbf{u}_h^i)-\frac{\mu}{\rho}K^{-1}\mathbf{u}_h^{i+1}\\
&\qquad-\frac{\beta}{\rho}|\mathbf{u}_h^{i+1}|\mathbf{u}_h^{i+1}+\mathbf{f}_h)\mathbf{z}_0\,d\mathbf{x}\Big]\\
&+\sum_{\kappa\in\mathcal{T}_h}\int_\kappa(\mathbf{f}-\mathbf{f}_h)\mathbf{z}_0\,d\mathbf{x}\\
&+\alpha\sum_{\kappa\in\mathcal{T}_h}\int_\kappa(\mathbf{u}_h^{i+1}-\mathbf{u}_h^i)\mathbf{z}_0\,d\mathbf{x}.
\end{aligned}\tag{42}$$

We decompose the fourth term of the left hand side as following

$$|\mathbf{u}|\mathbf{u}-|\mathbf{u}_h^{i+1}|\mathbf{u}_h^{i+1}=|\mathbf{u}|(\mathbf{u}-\mathbf{u}_h^{i+1})+(|\mathbf{u}|-|\mathbf{u}_h^{i+1}|)\mathbf{u}_h^{i+1},$$

and, use the property 2.1, the relation (4) and the schwarz inequality to get the following:

$$\begin{aligned}
&\frac{\mu K_m}{\rho}\|\mathbf{z}_0\|^2_{L^2(\Omega)}+c_m\left\|\mathbf{u}-\mathbf{u}_h^{i+1}\right\|^3_{L^3(\Omega)}\\
&\le\frac{\mu K_M}{\rho}\|\mathbf{z}_0\|_{L^2(\Omega)}\|\mathbf{v}_r\|_{L^2(\Omega)}\\
&\quad+\frac{\beta}{\rho}\|\mathbf{u}-\mathbf{u}_h^{i+1}\|_{L^3(\Omega)}(\|\mathbf{u}\|_{L^6(\Omega)}\\
&\quad+\|\mathbf{u}_h^{i+1}\|_{L^6(\Omega)})\|\mathbf{v}_r\|_{L^2(\Omega)}\\
&\quad+\sum_{\kappa\in\mathcal{T}_h}\|-\alpha(\mathbf{u}_h^{i+1}-\mathbf{u}_h^i)-\frac{\mu}{\rho}K^{-1}\mathbf{u}_h^{i+1}\\
&\qquad\qquad-\frac{\beta}{\rho}|\mathbf{u}_h^{i+1}|\mathbf{u}_h^{i+1}+\mathbf{f}_h\|_{L^2(\kappa)}\|\mathbf{z}_0\|L^2(\kappa)\\
&\quad+\sum_{\kappa\in\mathcal{T}_h}\|\mathbf{f}-\mathbf{f}_h\|_{L^2(\kappa)}\|\mathbf{z}_0\|_{L^2(\kappa)}\\
&\quad+\alpha\sum_{\kappa\in\mathcal{T}_h}\|\mathbf{u}_h^{i+1}-\mathbf{u}_h^i\|_{L^2(\kappa)}\|\mathbf{z}_0\|_{L^2(\kappa)}.
\end{aligned}\tag{43}$$

We use Lemma 4.1 and the decomposition $ab\le\frac{1}{2\varepsilon}a^2+\frac{1}{2}\varepsilon b^2$ for all the terms containing $b=\|\mathbf{z}_0\|_{L^2(\Omega)}$ (resp. $\|\mathbf{u}-\mathbf{u}_h^{i+1}\|_{L^3(\Omega)}$) in the right hand side of Equation (43), with ε sufficiently small such that all the terms of $\|\mathbf{z}_0\|_{L^2(\Omega)}$ (resp. $\|\mathbf{u}-\mathbf{u}_h^{i+1}\|_{L^3(\Omega)}$) in the right hand side will be absorbed by the term $\frac{\mu K_m}{2\rho}\|\mathbf{z}_0\|^2_{L^2(\Omega)}$ (resp. $c_m\|\mathbf{u}-\mathbf{u}_h^{i+1}\|_{L^3(\Omega)}$) of the left hand side of (43). We then get by taking the square root of the inequality, the bound

$$\begin{aligned}
&\|\mathbf{z}_0\|_{L^2(\Omega)}+\left\|\mathbf{u}-\mathbf{u}_h^{i+1}\right\|^{3/2}_{L^3(\Omega)}\\
&\le\overline{C}\Big(\|\mathbf{v}_r\|_{L^2(\Omega)}+\sum_{\kappa\in\mathcal{T}_h}\|\mathbf{f}-\mathbf{f}_h\|_{L^2(\kappa)}\\
&\qquad+\sum_{\kappa\in\mathcal{T}_h}\|\mathbf{u}_h^{i+1}-\mathbf{u}_h^i\|_{L^2(\kappa)}\\
&\qquad+\sum_{\kappa\in\mathcal{T}_h}\|-\frac{\mu}{\rho}K^{-1}\mathbf{u}_h^{i+1}-\alpha(\mathbf{u}_h^{i+1}-\mathbf{u}_h^i)\\
&\qquad\qquad-\frac{\beta}{\rho}|\mathbf{u}_h^i|\mathbf{u}_h^{i+1}+\mathbf{f}_h\|_{L^2(\kappa)}\Big),
\end{aligned}\tag{44}$$

where $\overline{C}$ is a constant depending on $(\mathbf{u},p)$. By using Relations (37) and (44), and the following inequality:

$$\|\mathbf{u}-\mathbf{u}_h^{i+1}\|_{L^2(\Omega)}\quad\le\quad\|\mathbf{z}_0\|_{L^2(\Omega)}+\|\mathbf{v}_r\|_{L^2(\Omega)}$$

we get the desired result. □

Remark 4.5. *Theorem 4.4 gives an upper bound for the error* $\mathbf{u}-\mathbf{u}_h^{i+1}=\boldsymbol{z}_0+\mathbf{v}_r$ *in* $L^2(\Omega)^d$ *and an upper bound of* $\mathbf{v}_r$ *in* X *which is a part of* $\mathbf{u}-\mathbf{u}_h^{i+1}$. *Furthermore, it gives an upper bound of* $\|\mathbf{u}-\mathbf{u}_h^{i+1}\|_{L^3(\Omega)}$ *but unfortunately, with the indicators to the power of* $2/3$.

The following theorem provides an upper bound for the error between the exact and numerical pressures in the $L^2(\Omega)$ norm, expressed in terms of the previously defined error indicators.

Theorem 4.6. *Under the assumptions of Theorem 4.4 and assume that* $\mathbf{f}\in L^2(\Omega)^d$, *then there exists a positive real number* i_1 *depending on* h *such that for all* $i\ge i_1$ *we have the following bound between the solutions* $(\mathbf{u},p)$ *of* (6) *and* $(\mathbf{u}_h^{i+1},p_h^{i+1})$ *of* (16)*:*

$$\begin{aligned}
&||p-p_h^{i+1}||_{L^2(\Omega)}\\
&\le C\Big[\sum_{\kappa\in\mathcal{T}_h}\left(\eta_{\kappa,i}^{(D_1)}+\eta_{\kappa,i}^{(L)}\right)\\
&\quad+\sum_{\kappa\in\mathcal{T}_h}\left(\|\mathbf{u}-\mathbf{u}_h^{i+1}\|_{L^2(\kappa)}+h_\kappa\|\boldsymbol{f}-\boldsymbol{f}_h\|_{L^2(\kappa)}\right)\Big],
\end{aligned}\tag{45}$$

where C *is a constant depending on* $(\mathbf{u},p)$.

Proof. Equation (26) can be rewritten as follows:

$$\begin{aligned}
&\int_\Omega (p-p_h^{i+1})\,\mathrm{div}\,\mathbf{v}\,d\mathbf{x}\\
&=\frac{\mu}{\rho}\int_\Omega K^{-1}(\mathbf{u}-\mathbf{u}_h^{i+1})\mathbf{v}\,d\mathbf{x}\\
&+\frac{\beta}{\rho}\int_\Omega (|\mathbf{u}|\mathbf{u}-|\mathbf{u}_h^{i+1}|\mathbf{u}_h^{i+1})\mathbf{v}\,d\mathbf{x}\\
&-\sum_{\kappa\in\mathcal{T}_h}\Big[\int_\kappa(-\alpha(\mathbf{u}_h^{i+1}-\mathbf{u}_h^i)-\frac{\mu}{\rho}K^{-1}\mathbf{u}_h^{i+1}\\
&\qquad -\frac{\beta}{\rho}|\mathbf{u}_h^{i+1}|\mathbf{u}_h^{i+1}-\nabla p_h^{i+1}+\mathbf{f}_h)(\mathbf{v}-\mathbf{v}_h)\,d\mathbf{x}\Big]\\
&-\frac{1}{2}\sum_{\kappa\in\mathcal{T}_h}\sum_{e\in\partial\kappa}\int_e[p_h^{i+1}\cdot\mathbf{n}]\,(\mathbf{v}-\mathbf{v}_h)\,d\mathbf{x}\\
&-\sum_{\kappa\in\mathcal{T}_h}\int_\kappa(\mathbf{f}-\mathbf{f}_h)(\mathbf{v}-\mathbf{v}_h)\,d\mathbf{x}\\
&-\alpha\sum_{\kappa\in\mathcal{T}_h}\int_\kappa(\mathbf{u}_h^{i+1}-\mathbf{u}_h^i)\mathbf{v}\,d\mathbf{x}.
\end{aligned}\tag{46}$$

Since $p_h^{i+1}-p$ belongs to $L^2(\Omega)$, owing to the inf-sup condition between $H_0^1(\Omega)^d$ and $L^2(\Omega)$ (Theorem 1, [33]), there exists $\mathbf{v}\in H_0^1(\Omega)^d$, such that

$$\int_\Omega (p_h^{i+1}-p)\,\mathbf{v}\,d\mathbf{x}=\|p_h^{i+1}-p\|^2_{L^2(\Omega)},\tag{47}$$

and

$$|\mathbf{v}|_{H^1(\Omega)^3}\le\frac{1}{\beta}\|p_h^{i+1}-p\|_{L^2(\Omega)}.\tag{48}$$

We choose this $\mathbf{v}$ and $\mathbf{v}_h=R_h\mathbf{v}$ in (46), use the relation (47), apply the Cauchy-Schwarz inequality, use the properties (24)-(25) of R_h, and infer by treating the second term of the right hand side as in (43),

$$\begin{aligned}
&\|p_h^{i+1}-p\|^2_{L^2(\Omega)}\\
&\le C\big(\|\mathbf{u}-\mathbf{u}_h^{i+1}\|_{L^2(\Omega)}\|\mathbf{v}\|_{L^2(\Omega)}\\
&+\frac{\beta}{\rho}\|\mathbf{u}-\mathbf{u}_h^{i+1}\|_{L^2(\Omega)}(\|\mathbf{u}\|_{L^6(\Omega)}\\
&+\|\mathbf{u}_h^{i+1}\|_{L^6(\Omega)})\|\mathbf{v}\|_{L^3(\Omega)}\\
&+\sum_{\kappa\in\mathcal{T}_h}\|\int_\kappa(-\alpha(\mathbf{u}_h^{i+1}-\mathbf{u}_h^i)-\frac{\mu}{\rho}K^{-1}\mathbf{u}_h^{i+1}\\
&\quad -\frac{\beta}{\rho}|\mathbf{u}_h^{i+1}|\mathbf{u}_h^{i+1}-\nabla p_h^{i+1}+\mathbf{f}_h\|_{L^2(\kappa)}h_\kappa|\mathbf{v}|_{H^1(w_\kappa)}\\
&\quad +\sum_{\kappa\in\mathcal{T}_h}\sum_{e\in\partial\kappa}\frac{1}{2}\|[p_h^{i+1}\cdot\mathbf{n}]\|_{L^2(e)}\,h_e^{1/2}|\mathbf{v}|_{H^1(w_e)}\\
&\quad +\sum_{\kappa\in\mathcal{T}_h}\|\mathbf{f}-\mathbf{f}_h\|_{L^2(e)}\,h_\kappa|\mathbf{v}|_{H^1(\kappa)}\\
&\quad +\alpha\sum_{\kappa\in\mathcal{T}_h}\|\mathbf{u}_h^{i+1}-\mathbf{u}_h^i\|_{L^2(e)}\,\|\mathbf{v}\|_{L^2(\kappa)}.
\end{aligned}\tag{49}$$

Then, by using the relation $\sum ab\le\big(\sum a^2\big)^{1/2}\big(\sum b^2\big)^{1/2}$, the inequality $\|\mathbf{v}\|_{L^s(\Omega)}\le C_s|\mathbf{v}|_{H^1(\Omega)}, 1\le s\le 6$, and Relation (48), we get the desired result. □

Remark 4.7. *The bounds* (40) *and* (45) *provide our a posteriori error estimates, quantifying the discrepancy between the exact solution* $(\mathbf{u},p)$ *of* (6) *and the numerical solution* $(\mathbf{u}_h^{i+1},p_h^{i+1})$ *of* (16) *in terms of the indicators* $\eta_{\kappa,i}^{(L)}$, $\eta_{\kappa,i}^{(D_1)}$ *and* $\eta_{\kappa,i}^{(D_2)}$.

Remark 4.8. *It is well known that when the Raviart–Thomas finite element is employed, the a posteriori error estimates for the Darcy (or Darcy–Forchheimer) problem are not optimal, [34], because the indicator cannot be locally bounded by the local error. However, if the data* **f** *are sufficiently smooth, optimality can be restored by adding an indicator obtained by taking the* ***curl*** *of equation* (1)*, [35]. This issue is currently under investigation and will be addressed in a forthcoming work.*

5 Numerical results

This section is devoted to numerical experiments that illustrate the behavior of Scheme (16). The implementation was carried out using the FreeFem++ software developed by [36]. Two test cases are examined: the first corresponds to an academic example for which the exact solution $(\mathbf{u},p)$ of Problem (6) is explicitly known; the second involves a more complicated geometry containing a reentrant corner.

5.1 First test case: convergence analysis

We consider the square domain $\Omega = (0,1)^2 \subset \mathbb{R}^2$, where each edge is uniformly partitioned into N segments. This produces a subdivision of Ω into $2N^2$ triangular.

The exact solution is taken in the form $(\mathbf{u}, p) = (\operatorname{curl}\psi, p)$, where the functions ψ and p are defined as follows:

$$\psi(x,y) = e^{-\delta((x-0.5)^2+(y-0.5)^2)} \tag{50}$$

and

$$p(x,y) = x(x-1)y(y-1). \tag{51}$$

We adopt the parameter values $\delta = 50$, $\gamma = \beta = 10$, and $\alpha = \mu = \rho = r_0 = 1$, with the permeability tensor set as $K = I$. Under this configuration, the source term $\mathbf{f}$ is computed according to the expressions derived from Equation (1). The choice of the parameter γ follows the recommendations in [3], [10]. Additionally, we use $N = 20$ for the initial mesh. We note that, given the selected exact solution, the divergence condition yields $b = \operatorname{div}\mathbf{u} = 0$ in Ω, and the pressure satisfies the homogeneous Dirichlet condition $p = 0$ on $\partial\Omega$.

For practical implementation on a given mesh, it is useful to compute the following error indicators:

$$\eta_i^{(D)} = \Big(\sum_{K\in\mathcal{T}_h} (\eta_{K,i}^{(D_1)})^2 + (\eta_{K,i}^{(D_2)})^2 \Big)^{\frac{1}{2}} \tag{52}$$

and

$$\eta_i^{(L)} = \Big(\sum_{K\in\mathcal{T}_h} ((\eta_{K,i}^{(L)})^2 \Big)^{\frac{1}{2}}. \tag{53}$$

The iterations are stopped following the criteria

$$\eta_i^{(L)} \le \tilde{\gamma}\eta_i^{(D)}. \tag{54}$$

We set $\tilde{\gamma} = 0.001$. For insights into the influence of the stopping criterion (54) with respect to the parameter $\tilde{\gamma}$, we refer to [37], [38], where this criterion was first introduced and analyzed.
We take the initial approximation $\mathbf{u}_h^0$ as the solution to the Darcy problem, obtained by setting $\beta = \alpha = 0$.
Furthermore, we evaluate the error:

$$Err = \sqrt{\frac{||\mathbf{u}_h^i - \mathbf{u}||^2_{L^2(\Omega)} + ||p_h^i - p||^2_{L^2(\Omega)}}{||\mathbf{u}||^2_{L^2(\Omega)} + ||p||^2_{L^2(\Omega)}}}$$

where $(\mathbf{u}, p)$ denotes the exact solution of Problem (6). This error serves as an indicator of the convergence behavior of the iterative algorithm (16). To compute the solution of the iterative problem (16), we employ the penalty method (see, [36]), which consists in solving the following modified problem:

$$\begin{cases} \forall \mathbf{v}_h \in X_h, \quad \displaystyle\int_\Omega \alpha(\mathbf{u}_h^{i+1} - \mathbf{u}_h^i)\mathbf{v}_h \, d\mathbf{x} \\ \displaystyle +\frac{\mu}{\rho}\int_\Omega K^{-1}\mathbf{u}_h^{i+1}\mathbf{v}_h \, d\mathbf{x} + \frac{\beta}{\rho}\int_\Omega |\mathbf{u}_h^i|\mathbf{u}_h^{i+1}\mathbf{v}_h \, d\mathbf{x} \\ \displaystyle -\int_\Omega p_h^{i+1} \operatorname{div}(\mathbf{v}_h) \, d\mathbf{x} = \int_\Omega \mathbf{f}\mathbf{v}_h \, d\mathbf{x}, \\ \\ \forall q_h \in M_h, \quad \displaystyle\int_\Omega q_h \operatorname{div}(\mathbf{u}_h^{i+1}) \, d\mathbf{x} \\ \displaystyle \qquad +\varepsilon_p \int_\Omega p_h^{i+1} q_h \, d\mathbf{x} = \int_\Omega b q_h \, d\mathbf{x}, \end{cases} \tag{55}$$

where $\varepsilon_p = 10^{-8}$.

For adaptive mesh refinement and coarsening, we utilize built-in routines in FreeFem++. The error indicators defined in (28) guide the mesh adaptation process through the following adaptive mesh algorithm:

(1) Given $\mathbf{u}_h^i$,
   (a) Solve the problem (16) to compute $\mathbf{u}_h^{i+1}$.
   (b) Calculate $\eta_i^{(D)}$ and $\eta_i^{(L)}$.
(2) If the stopping criterion (54) is met, proceed to step (3); otherwise, update $\mathbf{u}_h^i := \mathbf{u}_h^{i+1}$ and return to step (1).
(3)
   (a) If $\eta_i^{(D)}$ is less than a prescribed error tolerance ε, the iteration process is stopped.
   (b) Otherwise, the mesh is adapted using the local indicators $\eta_{K,i}^{(D)}$.
(4) Set $i = i + 1$ and go to (1).

In Figure 1, we illustrate the evolution of the mesh throughout the iterations (initial mesh, second, and fourth refinement levels). It is evident that the mesh becomes increasingly refined in regions where higher resolution is required to accurately capture the solution's behavior.
Next, we analyze the error curves by comparing the exact and numerical solutions obtained using both uniform and adaptive mesh refinement strategies. Figure 2 presents, in logarithmic scale, the global error Err plotted against the total number of degrees of freedom $Tdof$. By "global," we refer to the combined error in both velocity and pressure. The

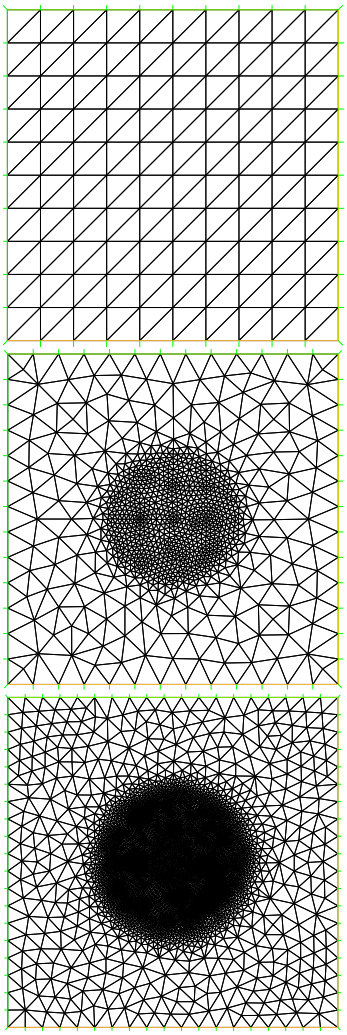

Figure 1: Evolution of the mesh during the refinement levels (up: initial, middle: second and down: fourth). (Source: created by the authors).

results clearly show that the adaptive method yields significantly lower errors than the uniform mesh approach, demonstrating the superior efficiency of adaptive refinement.

5.2 Second test case

In this section, we present numerical results for a more complex geometry (containing a reentrant corner, see Figure 3), using Problem (6) and the numerical scheme (16). For all numerical experiments reported here, we set:

$$f = \begin{cases} 0 & \text{if } y > 1, \\ -2 & \text{if } y <= 1, \end{cases}$$

and

$$K^{-1} = \begin{pmatrix} k_{11} & k_{12} \\ k_{21} & k_{22} \end{pmatrix}$$

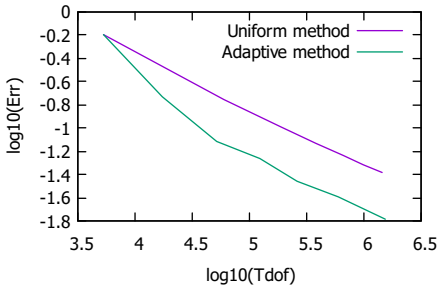

Figure 2: Comparison of the errors Err with respect to the total number of degrees of freedom $Tdof$ in logarithmic scale (First test case).
(Source: created by the authors).

where $k_{11} = 2 + \sin(\pi x)\sin(\pi y)$, $k_{12} = k_{21} = 0.2x$ and $k_{22} = 3 + \sin(\pi x)\sin(\pi y)$.

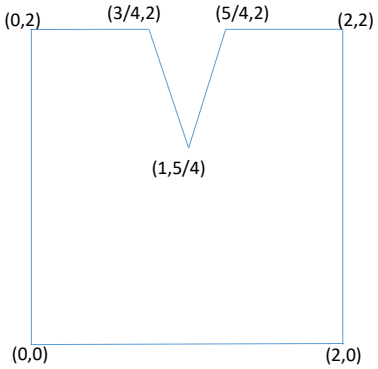

Figure 3: Geometry. (Source: created by the authors).

Figure 4 illustrates the evolution of the mesh throughout the iterations, showing the initial mesh as well as the results after the second and third refinement levels. In addition, Figure 5 presents, in logarithmic scale, a comparison of the error indicators $EtaD = \eta^D$ with respect to the total number of degrees of freedom $Tdof$ between the uniform and adaptive methods. In order to better compare the uniform and adaptive mesh methods, Table 1 illustrates the corresponding errors η^D with respect to the total number of degrees of freedom $Tdof$. We also note here that the adaptive method is more efficient than the uniform one.

6 Conclusion and perspective

In this paper, we have investigated the *a posteriori* error estimates associated with the iterative algorithm introduced in [6], for the Darcy–Forchheimer problem with pressure boundary conditions. The error between the exact solution $(\mathbf{u}, p)$ of Problem (6) and the numerical solution obtained from the iterative scheme (16) is controlled by two types of indicators: one measuring the discretization error and

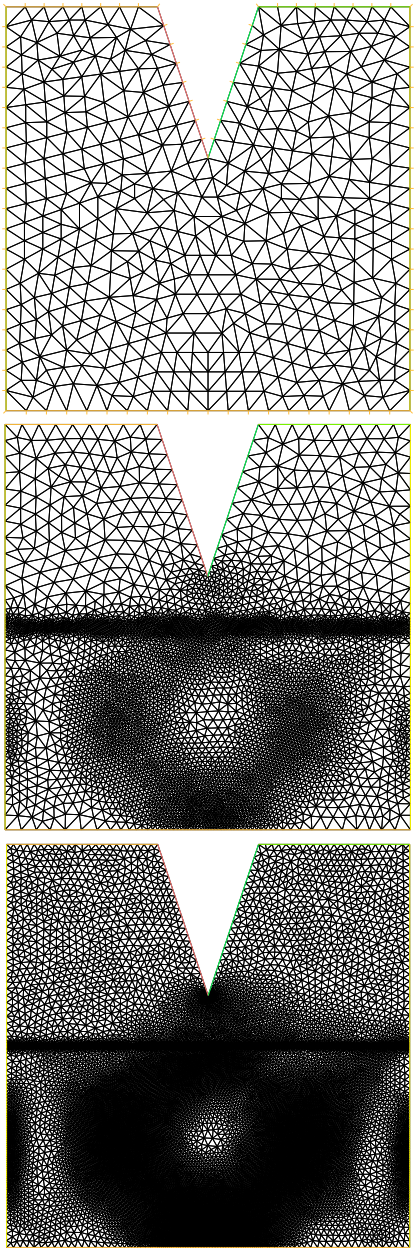

Figure 4: Evolution of the mesh during the refinement levels (up: initial, middle: second and down: third). (Source: created by the authors).

the other capturing the iteration error. Moreover, the numerical experiments demonstrated the efficiency of the adaptive mesh refinement strategy guided by the derived *a posteriori* error estimators.
Natural perspectives of this work can be summarized as follows:

1. Studying the optimality of the *a posteriori* error estimates addressed in this work.
2. Coupling system (1)–(4) with the heat equation or the concentration equation by studying the case where the term source **f** depends on the concentration.

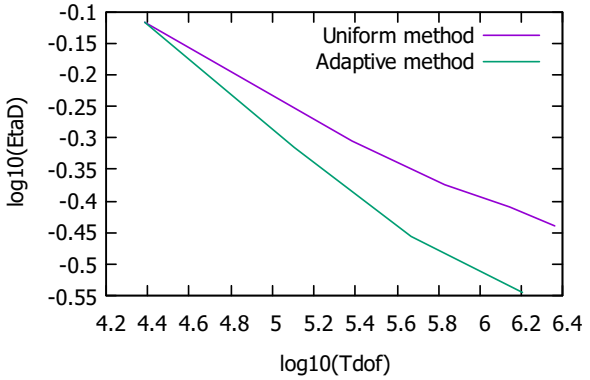

Figure 5: Comparison of the error indicators $EtaD = \eta^D$ with respect to the total number of degrees of freedom $Tdof$ in logarithmic scale for the second case. (Source: created by the authors).

Table 1: The error η^D with respect to the total number of degrees of freedom $Tdof$ in logarithmic scale for the uniform and adaptive mesh methods. (Source: created by the authors).

Uniform mesh method				
log10(Tdof)	4.38	5.38	5.83	6.15
log10(η^D)	-0.117	-0.305	-0.374	-0.410
Adaptive mesh method				
log10(Tdof)	4.38	5.10	5.66	6.20
log10(η^D)	-0.117	-0.315	-0.455	-0.544

References:

[1] Girault V., Wheeler M.F., Numerical discretization of a Darcy-Forchheimer model, *Numer. Math. 110(2), 161-198 (2008).*

[2] Lopez H., Molina B., Jose J.S., Comparison between different numerical discretizations for a Darcy-Forchheimer model, *Electron. Trans. Numer. Anal. 34, 187-203 (2009).*

[3] Sayah T., Semaan G., Triki F., Finite element methods for the Darcy-Forchheimer problem coupled with the convection-diffusion-reaction problem, *ESAIM Math. Model. Numer. Anal. 55(6), 2643-2678, (2021).*

[4] Pan H., Rui H., Mixed Element Method for Two-Dimensional Darcy-Forchheimer Model, *J. Sci. Comput. 52, 563-587, (2012).*

[5] Salas J.J., Lopez H., Molina B., An analysis of a mixed finite element method for

a Darcy-Forchheimer model, *Mathematical and Computer Modelling 57, 2325-2338 (2013).*

[6] Al Dbaissy R. and Sayah T., Iterative Scheme for the Darcy-Forchheimer Problem with Pressure Boundary Condition, *WSEAS Transactions on Heat and Mass Transfer, 19, (2024).*

[7] Caucao S, N.Gatica G, Oyarzua R and Sandoval F, Residual-based *a posteriori* error analysis for the coupling of the navier-stokes and darcy-forchheimer equations, *ESAIM:M2AN, 55, 659-697, (2021).*

[8] Sayah T., A posteriori error estimates for the Brinkman-Darcy-Forchheimer problem, *Computational and Applied Mathematics, 40, 256, (2021).*

[9] Sayah T., Semaan, Triki F., A Posteriori Error estimates for Darcy-Forchheimer's Problem, *Computational Methods in Applied Mathematics, 23 (2), 517-544, (2023).*

[10] Sayah T., Semaan G., Triki F., A Posteriori error estimates for Darcy-Forchheimer's problem coupled with the convection-diffusion-reaction equation, *International Journal of Numerical Analysis and Modeling, 21 (1), 65–103, (2024).*

[11] Alejandro Allendes A., Campa G. and Otarola E., Numerical Discretization of a Darcy-Forchheimer Problem Coupled with a Singular Heat Equation, *SIAM Journal on Scientific Computing, 45(5), (2023).*

[12] Aghaei-Jouybari, M., Seo, J.-H., Pinto, S., Cattafesta, L., Meneveau, C., Mittal, R., Extended Darcyâ€“Forchheimer law including inertial flow deflection effects. Journal of Fluid Mechanics, 980, A13. doi:10.1017/jfm.2023.1083 (2024)

[13] Akyildiz F.T., Alshammari F.S. and Tunç C., Novel Numerical Investigations of Some Problems Based on the Darcyâ€“Forchheimer Model and Heat Transfer, *Mathematics, 12(11), (2024).*

[14] Dehghan M., Gharibi Z., A fully mixed virtual element method for Darcyâ€“Forchheimer miscible displacement of incompressible fluids appearing in porous media, IMA Journal of Numerical Analysis, Volume 44, Issue 2, March 2024, Pages 797â€“835

[15] Granero-BelinchÃ³n R.and Scrobogna S., Asymptotic models for free boundary flow in porous media. Physica D: Nonlinear Phenomena. 392, 1-16, (2019).

[16] Grillo A. and Carfagnay M. and Federicoz S., The Darcy-Forchheimer Law for Modelling Fluid Flow in Biological Tissues *Theoretical and Applied Mechanics, 41, 283-322, (2014).*

[17] Huang J., Yue Z., Zhang J., Fu K., Feng X., Numerical discretization of a Darcyâ€“Forchheimer flow with variable density and heat transfer, *Journal of Computational and Applied Mathematics, 457, (2025).*

[18] Li A., Huang J,, Liu W., Wei H., Yi N., A characteristic block-centered finite difference method for Darcyâ€“Forchheimer compressible miscible displacement problem, *Journal of Computational and Applied Mathematics, 413, (2022).*

[19] Lychagin V.V., On Darcyâ€“Forchheimer Flows in Porous Media, *Lobachevskii J Math 43, 2793â€“2796 (2022).*

[20] Winter R., Valsamidou A., Class H., Flemisch B., A Study on Darcy versus Forchheimer Models for Flow through Heterogeneous Landfills including Macropores, *Water; 14(4):546, (2022).*

[21] Pamuk M.T., Numerical Simulation of Pressure Loss in Porous Media in Oscillating Flow, *WSEAS Transactions on Fluid Mechanics, 13, pp. 37-44, (2018).*

[22] Grosan T., Pop I., Patrulescu, F. O., Transfer Phenomena in Non-Darcy Bidisperse Porous Media, *WSEAS Transactions on Heat and Mass Transfer, 14, 147-152, (2019).*

[23] Li S., Khan M., Ali S., Ullah Khan S., Althobaiti S., Khan I., Alqurashi F., Kchaou M., Influence of variable fluid properties on mixed convective Darcyâ€“Forchheimer flow relation over a surface with Soret and Dufour spectacle. Open Physics, 22(1), 20240010 (2024).

[24] Salawu S. O., Analysis of Third-Grade Heat Absorption Hydromagnetic Exothermic Chemical Reactive Flow in a Darcy-Forchheimer Porous Medium with Convective Cooling, *WSEAS Transactions on mathematics, 17, 280-289, (2018).*

[25] Tsuji K., Fujioka S., Morikawa D.S. et al. A reliable SPH(2) formulation for Darcyâ€“Forchheimerâ€“Brinkman equation using a density-based particle shifting in the ALE description. Comp. Part. Mech. (2024).

[26] Zhang W. and Mehrabian A., Nonlinear and non-local analytical solution for Darcyâ€“Forchheimer flow through a deformable porous inclusion within a semi-infinite elastic medium, *Journal of Fluid Mechanics, 911, (2021).*

[27] Fabrie P., Regularity of the solution of Darcy-Forchheimer's equation. *Nonlinear Anal. Theory Methods, 13, 1025-1045, (1989).*

[28] Ciarlet P. G., Basic error estimates for elliptic problems,*In Handbook of Numerical Analysis, Vol. II, Handbook of Numerical Analysis, pages 17-351. North-Holland, Amsterdam, (1991).*

[29] Ern A. and Guermond J.L., Theory and Practice of Finite Elements, *Springer Science & Business Media, 159, (2004).*

[30] Raviart P.-A., Thomas J.M., A mixed finite element method for 2-nd order elliptic problems, *Mathematical Aspects of the Finite Element Method. Lecture Notes in Mathematics, vol. 606, 292-315, Springer, Berlin (1977).*

[31] Brezzi, F., Douglas, J. Jr., Marini, L.D., Two families of mixed finite elements for second order elliptic problems, *Numer. Math. 47(2), 217-235 (1985).*

[32] Clément P., Approximation by finite element functions using local regularization, *RAIRO Anal. Numér. 9, R2,77-84, (1975).*

[33] Braack M. and Richter T., Inf-sup condition for Stokes with outflow condition, *arXiv, https://arxiv.org/abs/2502.02146, (2025).*

[34] Braess D. and Verfurth. R., A posteriori error estimators for the Raviart-Thomas element, *SIAM J. Numer. Anal., 33(6), 2431–2444, (1996).*

[35] Chen W. and Wang Y., *A posteriori estimate for the $h(\mathrm{div}, w)$ conforming mixed finite element for the coupled Darcy-Stokes system, Journal of Computational and Applied Mathematics, 255, 502–516, (2014).*

[36] Hecht F., New development in FreeFem++, *Journal of Numerical Mathematics, 20, 251–266, (2012).*

[37] El Alaoui L., Ern A.,Vohralík M., Guaranteed and robust a posteriori error estimates and balancing discretization and linearization errors for monotone nonlinear problems, *Computable Methods in Applied Mechanics and Engineering **200**, 2782-2795, (2011).*

[38] Ern A., Vohralík M., Adaptive inexact Newton methods with a posteriori stopping criteria for nonlinear diffusion PDEs, *SIAMJ. Sci. Comput. **35**, **4**, A1761-A1791, (2013).*

Contribution of Individual Authors to the Creation of a Scientific Article (Ghostwriting Policy)

The authors equally contributed in the present research, at all stages from the formulation of the problem to the final findings and solution.

Sources of Funding for Research Presented in a Scientific Article or Scientific Article Itself

No funding was received for conducting this study.

Conflict of Interest

The authors have no conflicts of interest to declare that are relevant to the content of this article.

Creative Commons Attribution License 4.0 (Attribution 4.0 International, CC BY 4.0)

This article is published under the terms of the Creative Commons Attribution License 4.0
https://creativecommons.org/licenses/by/4.0/deed.en_US